

Abstract

This work presents a physics-infused reduced-order modeling (PIROM) framework towards the design, analysis, and optimization of ablating hypersonic thermal protection systems (TPS).

1 Introduction

At hypersonic speeds, aerospace vehicles experience extreme aero-thermal environments that requires specialized thermal protection systems (TPS) to shield internal sub-structures, electronics, and possibly crew members from the intense aerodynamic heating. The TPS is often composed of ablating materials – a high-temperature capable fibrous material injected with a resin that fills the pore network and strengthens the composite [Amar2016]. The TPS design promotes the exchange of mass through thermal and chemical reactions (i.e., pyrolysis), effectively mitigating heat transfer to the sub-structures.

As a result, accurate prediction for the ablating TPS response under extreme hypersonic heating becomes fundamental to ensuring survivability, performance, and safety of hypersonic vehicles. Not only is it necessary to assess the performance of the thermal management systems, but also the shape changes of the vehicle’s outer surface induced by the ablating material, and its impact on the aerodynamics, structural integrity, and controllability. Unfortunately, high-fidelity simulations of ablating TPS remains a formidable challenge both theoretically and computationally.

On the theoretical side, the thermo-chemical reactions, coupled with the irregular pore network structure, translate into simplifying assumptions to reduce non-linearities, and make the resulting equations more amenable for engineering application and design analysis [x]. For instance, one of the most notable codes is the one-dimensional CMA code that was developed by Aerotherm Corporation in the 1960s [Howard2015]. Despite its practical use in...

Another example is the CHarring Ablator Response (CHAR) ablation code, which ignores elemental decompositions of the pyrolyzing gases, assumes the gases to be a mixture of perfect gases in thermal equilibrium, and assumes no reaction or condensation with the porous network [?].

theoretically:

computationally:

2 Modeling of Ablating Thermal Protection Systems

This section presents the problem of modeling ablation for a non-decomposing TPS as a parametrized system of coupled non-linear PDEs. The ablation physics is decomposed into heat conduction and mesh motion, which are governed by the energy and pseudo-elasticity PDEs, respectively. Predictions for the ablating TPS response computed based on two models: (1) a high-fidelity FOM based on discontinuous Galerkin FEM (DG-FEM), and (2) an RPM based on the LCM. The mathematical details for the governing equations, FOM, and RPM, are provided next.

2.1 Governing Equations

Heat Conduction Consider a generic domain $\Omega \subset \mathbb{R}^d$, $d = 2$ or 3 , illustrated in Fig. 1. Let $\partial\Omega = \Gamma_q \cup \Gamma_T$ and $\Gamma_q \cap \Gamma_T = \emptyset$, where a Neumann $q_b(x, t)$ boundary condition is prescribed on the Γ_q boundary, and a Dirichlet $T_b(x, t)$ boundary condition is prescribed on the boundary Γ_T . The ablation is modeled as mesh motion, and occurs only on the heated boundary Γ_q . Ablating effects on the energy equation are handled using the Arbitrary Lagrangian-Eulerian (ALE) description. The ALE establishes that mesh displacements $w(x, t) \in \mathbb{R}^d$ and velocities $v(x, t) \in \mathbb{R}^d$ evolve independently of the physical material’s displacements, which are set to zero [CITE].



Figure 1: General domain Ω with prescribed Neumann and Dirichlet boundary conditions on Γ_q and Γ_T . Mesh displacement $w(x, t)$ occurs on the Γ_q boundary.

The transient heat conduction is described by the energy equation,

$$\rho c_p \left(\frac{\partial T}{\partial t} - v(x, t) \cdot \nabla T \right) - \nabla \cdot (\mathbf{k} \nabla T) = \mathcal{Q}(x, t), \quad x \in \Omega \quad (1a)$$

$$-\mathbf{k} \nabla T \cdot \mathbf{n} = q_b(x, t), \quad x \in \Gamma_q \quad (1b)$$

$$T(x, t) = T_b(x, t), \quad x \in \Gamma_T \quad (1c)$$

$$T(x, 0) = T_0(x), \quad x \in \Omega \quad (1d)$$

where the density ρ is constant, while the heat capacity c_p and thermal conductivity $\mathbf{k} \in \mathbb{R}^{d \times d}$, are temperature dependent. In the order they appear, the terms in eq. (1a) include, the unsteady energy storage, heat conduction, temperature advection due to mesh motion, and source terms due to boundary conditions.

Mesh Motion The mesh motion is described by the pseudo-elasticity equation,

$$\nabla \cdot \sigma(w) = 0 \quad (2a)$$

$$w(x, t) = w_q(x, t), \quad x \in \Gamma_q \quad (2b)$$

$$w(x, t) = 0, \quad x \notin \Gamma_q \quad (2c)$$

$$w(x, 0) = \mathbf{0} \quad (2d)$$

where the stress tensor σ is related to the strain tensor $\epsilon(w)$ through Hooke's law,

$$\sigma(w) = \mathbb{D} : \epsilon(w)$$

where \mathbb{D} is the constitutive operator, “:” is the double contraction of tensors, and ϵ is the symmetric strain tensor given by,

$$\epsilon(\mathbf{w}) = \frac{1}{2} (\nabla \mathbf{w} + \nabla \mathbf{w}^T)$$

For instance, an isotropic material assumption results in,

$$\boldsymbol{\sigma} = \lambda (\nabla \cdot \mathbf{w}) \mathbf{I} + 2\mu \boldsymbol{\epsilon}(\mathbf{w})$$

where λ and μ are Lamé constants that are arbitrarily selected to model the mesh motion. The “material” properties λ and μ can be chosen to tailor the mesh deformation and need not represent the actual material being modeled [Amar2016](#).

The boundary conditions for the energy equation includes a heated surface (eq. (1b)) and a constant-temperature surface (eq. (1c)). The boundary conditions for the pseudo-elasticity equation are a function of the surface temperature $T_q(x, t)$ for $x \in \Gamma_q$ using a B’ table. The B’ table....

$$\mathbf{w}_q(x, t) = \int_0^t \mathbf{v}(x, \tau) d\tau = \int_0^t \mathbf{f}(T_q(x, \tau)) d\tau \quad (3)$$

2.2 Full-Order Model: Finite-Element Method

To obtain the full-order numerical solution, the governing equation is spatially discretized using variational principles of Discontinuous Galerkin (DG) to result in a high-dimensional system of ordinary differential equations (ODEs). Note that the choice of DG approach here is mainly for theoretical convenience in the coarse-graining formulation, and is exclusively performed on the energy equation as the quantities of interest correspond to the ablating surface temperatures. In Sec. [x](#), the high-fidelity ablating TPS solution is performed using standard FEM for both the energy and elasticity equations, and the equivalence between DG and standard FEM is noted upon their convergence.

Consider a conforming mesh partition domain, where each element belongs to one and only one component. Denote the collection of all M elements as $\{E_i\}_{i=1}^M$. In an element E_i , its shared boundaries with another element E_j , Neumann BC, and Dirichlet BC are denoted as e_{ij} , e_{iq} , and e_{iT} , respectively. Lastly, $|e|$ denotes the length ($n_d = 2$) or area ($n_d = 3$) of a component boundary e .

For the i -th element, use a set of P trial functions, such as polynomials, to represent the temperature distribution,

$$T^{(i)}(x, t) = \sum_{l=1}^P \phi_l^{(i)}(x) u_l^{(i)} \equiv \boldsymbol{\phi}^{(i)}(x)^T \mathbf{u}^{(i)}(t), \quad i = 1, 2, \dots, M \quad (4)$$

By standard variational processes, e.g., [Cohen2018](#), the element-wise governing equation is denoted as,

$$\mathbf{A}^{(i)} \dot{\mathbf{u}}^{(i)} = (\mathbf{B}^{(i)} + \mathbf{C}^{(i)}(t)) \mathbf{u}^{(i)} + \sum_{j \in \mathcal{N}_i \cup \{T_b\}} \left(\mathbf{B}_{ij}^{(i)} \mathbf{u}^{(i)} + \mathbf{B}_{ij}^{(j)} \mathbf{u}^{(j)} \right) + \mathbf{f}^{(i)}(t), \quad \text{for } i = 1, 2, \dots, M \quad (5)$$

which is collected as the following ODE for the all the elements in the mesh,

$$\mathbf{A}(\mathbf{u}) \dot{\mathbf{u}} = [\mathbf{B}(\mathbf{u}) + \mathbf{C}(t, \mathbf{u})] \mathbf{u} + \mathbf{f}(t) \quad (6)$$

where $\mathbf{u} = [\mathbf{u}^{(1)}, \mathbf{u}^{(2)}, \dots, \mathbf{u}^{(M)}]^T \in \mathbb{R}^{MP}$ includes all the DG variables, $\mathbf{f} \in \mathbb{R}^{MP}$ is the external forcing, and the system matrices \mathbf{A} , \mathbf{B} , and \mathbf{C} are the matrices due to heat capacity, heat conduction, and temperature advection due to mesh motion, respectively. A detailed derivation of eqs. (5) and (6) and their matrices is provided in Appendix [?].

2.3 Reduced-Physics Model

The RPM for predicting the response of the ablating TPS consists of two components: (1) the LCM, and (2) tabulated data for ablating velocity as a function of surface temperature. The LCM is described as a first-order system of ODEs for predicting the average temperatures inside the ablating TPS, and provides a low-fidelity under-estimation for the ablating surface temperature. The temperature prediction from LCM is used in a B’ table to determine the surface recession velocity, from which the displacements are obtained through integration.

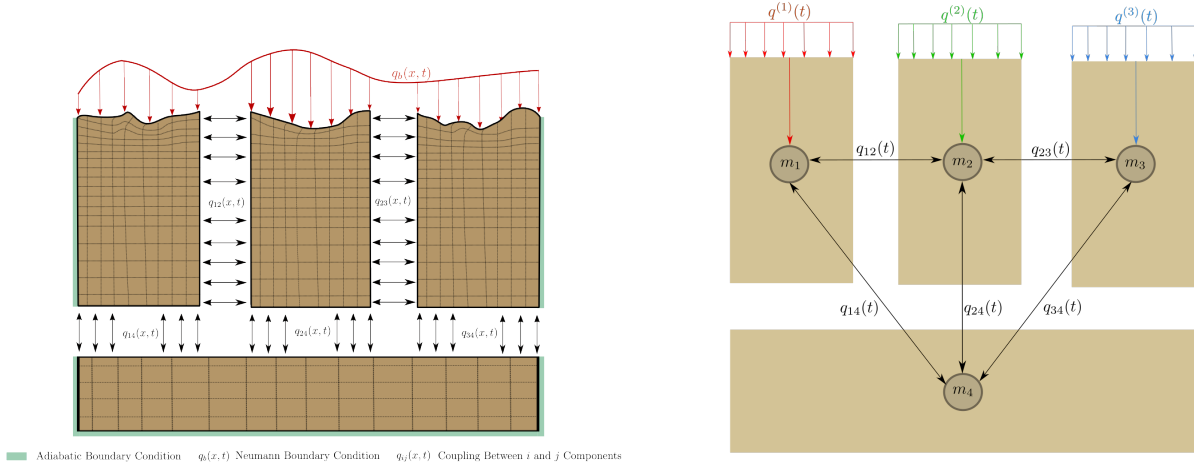


Figure 2: Partition of the TPS into three ablating and one non-ablating components with the corresponding lumped-mass representation

2.3.1 Lumped Capacitance Model

The main results regarding the LCM are provided in this section; details of the implementation for the TPS in Fig. 2 are provided in Appendix A. The LCM is a classical physics-based low-order model for predicting the temporal variation of average temperature in multiple interconnected components **INCROPERA**. The LCM is derived at the component level from a point of view of energy conservation, and leads to the following system of ODEs for the average temperatures on the components,

$$\bar{\mathbf{A}} \dot{\bar{\mathbf{u}}} = \bar{\mathbf{B}}(\bar{\mathbf{u}}) \bar{\mathbf{u}} + \bar{\mathbf{f}}(t) \quad (7)$$

where,

$$\bar{\mathbf{u}} = [\bar{u}^{(1)}, \bar{u}^{(2)}, \dots, \bar{u}^{(N)}]^T \in \mathbb{R}^N \quad (8a)$$

$$\bar{\mathbf{f}} = [\bar{f}^{(1)}, \bar{f}^{(2)}, \dots, \bar{f}^{(N)}]^T \in \mathbb{R}^N \quad (8b)$$

includes the average temperatures $\bar{\mathbf{u}}$ and forcing inputs $\bar{\mathbf{f}}$ for the N components. For $i, j = 1, 2, \dots, N$ the (i, j) -th elements of the $\bar{\mathbf{A}} \in \mathbb{R}^{N \times N}$, $\bar{\mathbf{B}} \in \mathbb{R}^{N \times N}$, and $\bar{\mathbf{f}} \in \mathbb{R}^N$ matrices are given by,

$$\bar{A}^{(i)} = \begin{cases} \int_{\Omega^{(i)}} \rho c_p d\Omega^{(i)}, & i = j \\ 0, & i \neq j \end{cases}, \quad \bar{B}_{ij} = \begin{cases} \sum_{j \in \mathcal{N}_i \cup \{T_b\}} \bar{B}_{ij}^{(i)}, & i = j \\ \bar{B}_{ij}^{(j)}, & i \neq j \end{cases}, \quad (9a)$$

$$\bar{f}^{(i)} = \begin{cases} |e_{iq}| \bar{q}^{(i)} + \frac{|e_{iT}|}{R_i} \bar{T}^{(i)}, & i = j \\ 0, & i \neq j \end{cases} \quad (9b)$$

where,

$$\bar{q}^{(i)} = \frac{1}{|e_{iq}|} \int_{e_{iq}} q_b de_{iq}, \quad \bar{T}^{(i)} = \frac{1}{|e_{iT}|} \int_{e_{iT}} T_b de_{iT}, \quad \bar{B}_{ij}^{(i)} = -\frac{|e_{ij}|}{R_{ij}}, \quad \bar{B}_{ij}^{(j)} = \frac{|e_{ij}|}{R_{ij}} \quad (10)$$

2.3.2 Surface Recession Velocity and Displacements

Using the predicted i -th average temperature $\bar{u}^{(i)}$ from LCM, the surface recession velocity and displacements are computed as,

$$\dot{w}^{(i)}(t) = h^{(i)}(\bar{u}^{(i)}), \quad w^{(i)}(t) = w^{(i)}(t_0) + \int_{t_0}^t h^{(i)}(\bar{u}^{(i)}) d\tau \quad (11)$$

where $h^{(i)}$ is a **x** fit to the B' tabulated data for the material. **Discussion of the B' tabulated data**. The B' table is pre-computed based on high-fidelity simulations of the ablation process for a one-dimensional slab of the material, and is independent of the TPS geometry and boundary conditions.

2.4 Summary of Modeling Approaches

The FOM (i.e., DG-FEM) and RPM (i.e., LCM) are two different but mathematically connected solution strategies. Specifically, the LCM in eq. (7) not only resembles the functional form of the DG model in eq. (6), but can be viewed as a special case of the latter, where the mesh partition is extremely coarse, and the trial and test functions are piece-wise constants. For example, consider the case where each component $\Omega^{(i)}$ is treated as one single element, and each element employs one constant basis function $\phi^{(i)} = 1$. The element-wise DG model in eq. (5) simplifies into a scalar ODE that ignores advection effects due to mesh motion,

$$\mathbf{A}^{(i)} = \bar{A}^{(i)}, \quad \mathbf{C}^{(i)} = 0, \quad \mathbf{B}_{ij}^{(i)} = -\sigma|e_{ij}|, \quad \mathbf{B}_{ij}^{(j)} = \sigma|e_{ij}|, \quad \mathbf{f}^{(i)} = |e_{iq}|\bar{q}^{(i)} + \sigma|e_{iT}|\bar{T}^{(i)} \quad (12)$$

Clearly, the LCM is a coarse zeroth-order DG model with the inverse of thermal resistance chosen as the element-wise penalty factors. Or conversely, the DG model is a refined version of LCM via *hp*-adaptation.

The FOM and RPM represent two extremes in the modeling fidelity and computational cost spectrum. On one hand, the FOM is the most accurate but computationally expensive to evaluate due to the fine mesh discretizations for both the temperature and displacement fields, leading to possibly millions of state variables. On the other hand, the RPM considers only the average temperature of the material as the state variable, considerably reducing the computational cost, but sacrificing local temperature information and thus neglecting higher-order effects due to mesh motion. Thus, neither the FOM nor the RPM is a universal approach for real-world analysis, design, and optimization tasks for ablating TPS, where thousands of high-fidelity model evaluations may be necessary. This issue motivates the development of the PIROM, which can achieve the fidelity of FOM at a computational cost close to the RPM, while maintaining the generalizability to model parameters.

3 Physics-Infused Reduced-Order Modeling

The formulation of PIROM for ablating TPS starts by connecting the FOM, i.e., DG-FEM, and the RPM, i.e., the LCM, via a coarse-graining procedure. This procedure pinpoints the missing dynamics in the LCM when compared to DG-FEM. Subsequently, the Mori-Zwanzig (MZ) formalism is employed to determine the model form for the missing dynamics in PIROM. Lastly, the data-driven identification of the missing dynamics in PIROM is presented.

3.1 Deriving the Reduced-Physics Model via Coarse-Graining

The LCM is derived from a full-order DG on a fine mesh via a projection process, i.e., coarse graining. This process constraints the trial function space of a full-order DF model to a subset of piece-wise constants, so that the variables \mathbf{u} , matrices \mathbf{A} , \mathbf{B} , and \mathbf{C} , and forcing vector \mathbf{f} are all approximated using a single state associated to the average temperature. The details of the projection are described next.

3.1.1 Coarse-Graining of States

Consider a DG model as in eq. (6) for M elements and an LCM as in eq. (7) for N components; clearly $M \gg N$.

A Implementation Details

A.1 Full-Order Model

To obtain the full-order numerical solution, the governing equation is spatially discretized using variational principles of Discontinuous Galerkin (DG) to result in a high-dimensional system of ordinary differential equations (ODEs). The DG-FEM model is written in an element-wise form, which is beneficial for subsequent derivations of the lower-order models. Note that the choice of DG approach here is mainly for theoretical convenience in the subsequent coarse-graining formulation. In the numerical results, the full-order TPS ablation simulations is computed using standard FEM instead, and the equivalence between DG and standard FEM is noted upon their convergence.

A.1.1 Domain Discretization

Consider a conforming mesh partition of the domain, as shown in Fig. **DOMAIN**, where each element belongs to one and only one component. Denote the collection of all M elements as $\{E_i\}_{i=1}^M$. To ease the description of the DG model, a graph structure is employed. The elements are treated as vertices, the set of which is denoted $\mathcal{V} = \{m\}_{m=1}^M$. Two neighboring elements, E_i and E_j , are connected by an edge (i, j) , and the shared boundary between them is denoted e_{ij} . The collection of all edges are denoted \mathcal{E} , and \mathcal{G} is referred to as a graph. In the graph, the edges are unidirected, meaning if $(i, j) \in \mathcal{E}$ then $(j, i) \in \mathcal{E}$. Furthermore, denote the neighbors of the i -th element as $\mathcal{N}_i = \{j | (i, j) \in \mathcal{E}\}$. Lastly, for the ease of notation, introduce two special indices: T for the boundary of an element that overlaps with the Dirichlet boundary condition, and similarly q for the Neumann boundary condition.

A.1.2 Weak Form of Discontinuous Galerkin Method

Choosing appropriate basis functions ϕ_k and ϕ_l and using the Interior Penalty Galerkin (IPG) scheme [?], the variational bilinear form for eq. (1a) is,

$$\sum_{i=1}^M a_{\epsilon,i}(\phi_k, \phi_l) = \sum_{i=1}^M L_i(\phi_k) \quad (13)$$

where ϵ is an user-specified parameter and,

$$a_{\epsilon,i}(\phi_k, \phi_l) = \int_{E^{(i)}} \left(\rho c_p \phi_k \frac{\partial \phi_l}{\partial t} + \nabla \phi_k \cdot (\mathbf{k} \nabla \phi_l) - \rho c_p \phi_k \mathbf{v} \cdot \nabla \phi_l \right) dE^{(i)} \quad (14a)$$

$$\begin{aligned} &= - \sum_{j \in \mathcal{N}_i \cup \{T_b\}} \int_{e_{ij}} \{ \mathbf{k} \nabla \phi_k \cdot \mathbf{n} \} [\phi_l] de_{ij} + \epsilon \sum_{j \in \mathcal{N}_i \cup \{T_b\}} \int_{e_{ij}} \{ \mathbf{k} \nabla \phi_l \cdot \mathbf{n} \} [\phi_k] de_{ij} \\ &+ \sigma \sum_{j \in \mathcal{N}_i \cup \{T_b\}} \int_{e_{ij}} [\phi_k] [\phi_l] de_{ij} \end{aligned} \quad (14b)$$

$$L_i(v) = \epsilon \sum_{j \in \mathcal{N}_i \cup \{T_b\}} \int_{e_{ij}} (\mathbf{k} \nabla \phi_l \cdot \mathbf{n}) T_b de_{ij} + \int_{e_{iq}} \phi_k q_b de_{iq} + \sigma \int_{e_{iT}} \phi_k T_b de_{iT} \quad (14c)$$

In the bi-linear form above, the notations $[]$ and $\{\}$ are respectively the jumps and averages at the boundary e_{ij} share by two elements E_i and E_j ,

$$[u] = u|_{E_i} - u|_{E_j}, \quad \{u\} = \frac{1}{2} \left(u|_{E_i} + u|_{E_j} \right), \quad \text{for } x \in e_{ij} = E_i \cap E_j$$

Furthermore, in the bi-linear form, the terms associated with σ are introduced to enforce the Dirichlet boundary conditions; σ is a penalty factor whose value can depend on the size of an element. Depending

on the choice of ϵ , the bi-linear form corresponds to symmetric IPG ($\epsilon = -1$), non-symmetric IPG ($\epsilon = 1$), and incomplete IPG ($\epsilon = 0$). All these schemes are consistent with the original PDE and have similar convergence rate with respect to mesh size. In the following derivations, the case $\epsilon = 0$ is chosen for the sake of simplicity.

A.1.3 Discontinuous Galerkin Model

Next, the DG-based model is written in an element-wise form. For the i -th element, use a set of P trial functions to represent the temperature as in eq. (4). Without loss of generality, the trial functions are assumed to be orthogonal, so that $\int_{E^{(i)}} \phi_k^{(i)}(x) \phi_l^{(i)}(x) dx = |E^{(i)}| \delta_{kl}$, where $|E^{(i)}|$ is the area ($n_d = 2$) or volume ($n_d = 3$) of the i -th element, and δ_{kl} is the Kronecker delta.

Using test functions same as trial functions, the dynamics $\mathbf{u}^{(i)}$ is obtained by evaluating the element-wise bi-linear forms,

$$a_{\epsilon,i}(\phi_k^{(i)}, T^{(i)}) = L_i(\phi_k^{(i)}), \quad k = 1, 2, \dots, P \quad (15)$$

The above procedure yields,

$$\mathbf{A}^{(i)} \dot{\mathbf{u}}^{(i)} = (\mathbf{B}^{(i)} + \mathbf{C}^{(i)}(t)) \mathbf{u}^{(i)} + \sum_{j \in \mathcal{N}_i \cup \{T_b\}} (\mathbf{B}_{ij}^{(i)} \mathbf{u}^{(i)} + \mathbf{B}_{ij}^{(j)} \mathbf{u}^{(j)}) + \mathbf{f}^{(i)}(t) \quad (16)$$

where for $k, l = 1, 2, \dots, P$,

$$[\mathbf{A}^{(i)}]_{kl} = \int_{E^{(i)}} \rho c_p \phi_k^{(i)} \phi_l^{(i)} dE^{(i)} \quad (17a)$$

$$[\mathbf{B}^{(i)}]_{kl} = - \int_{E^{(i)}} (\nabla \phi_k^{(i)}) \cdot (\mathbf{k} \nabla \phi_l^{(i)}) dE^{(i)} \quad (17b)$$

$$[\mathbf{C}^{(i)}]_{kl} = \int_{E^{(i)}} \rho c_p \phi_k^{(i)} \mathbf{v}^{(i)} \cdot \nabla \phi_l^{(i)} dE^{(i)} \quad (17c)$$

$$[\mathbf{B}_{ij}^{(i)}] = \int_{e_{ij}} \left\{ \mathbf{k} \nabla \phi_k^{(i)} \cdot \hat{n} \right\} \phi_l^{(i)} - \sigma [\phi_k^{(i)}] \phi_l^{(i)} de_{ij} \quad (17d)$$

$$[\mathbf{B}_{ij}^{(j)}] = \int_{e_{ij}} - \left\{ \mathbf{k} \nabla \phi_k^{(i)} \cdot \hat{n} \right\} \phi_l^{(j)} + \sigma [\phi_k^{(i)}] \phi_l^{(j)} de_{ij} \quad (17e)$$

$$[\mathbf{f}^{(i)}]_k = \int_{e_{iq}} \phi_k^{(i)} q_b de_{iq} + \sigma \int_{e_{iT}} \phi_k^{(i)} de_{iT} \quad (17f)$$

Note that the matrices $\mathbf{A}^{(i)}$, $\mathbf{C}^{(i)}$, and \mathbf{B}_{ij} depend on ρ , c_p , and \mathbf{k} , respectively, and hence can be a non-linear function of \mathbf{u} . Since the trial functions are orthogonal, if ρc_p is constant within an element, $\mathbf{A}^{(i)}$ is diagonal; otherwise, \mathbf{A}_i is symmetric and positive definite as $\rho c_p > 0$.

For compactness, the element-wise model in eq. (16) is also written in matrix form,

$$\mathbf{A}(\dot{\mathbf{u}}) = [\mathbf{B}(\mathbf{u}) + \mathbf{C}(t, \mathbf{u})] \mathbf{u} + \mathbf{f}(t) \quad (18)$$

where $\mathbf{u} = [\mathbf{u}^{(1)}, \mathbf{u}^{(2)}, \dots, \mathbf{u}^{(M)}]^T \in \mathbb{R}^{MP}$ includes all DG variables, $\mathbf{f} = [\mathbf{f}^{(1)}, \mathbf{f}^{(2)}, \dots, \mathbf{f}^{(M)}]^T \in \mathbb{R}^{MP}$, \mathbf{A} and \mathbf{C} are matrices of M diagonal blocks whose i -th blocks are $\mathbf{A}^{(i)}$ and $\mathbf{C}^{(i)}$, and \mathbf{B} is a matrix of $M \times M$ blocks whose (i, j) -th block is,

$$\mathbf{B}_{ij} = \begin{cases} \mathbf{B}^{(i)} + \sum_{j \in \mathcal{N}_i \cup \{T_b\}} \mathbf{B}_{ij}^{(i)}, & i = j \\ \mathbf{B}_{ij}^{(j)}, & i \neq j \end{cases} \quad (19)$$

The dependency of \mathbf{A} , \mathbf{B} , and \mathbf{C} on \mathbf{u} is explicitly noted in eq. (18), which is the source of non-linearity in the current TPS problem. Moreover, the mesh velocity \mathbf{v} varies with space and time, and thus the advection matrix \mathbf{C} varies with time as a function of q_b .

A.2 Lumped Capacitance Model

The following assumptions are employed: (1) the temperature in component (i) is described by a scalar time-varying average temperature $\bar{u}^{(i)}$, (2) between neighboring components (i) and (j) the heat flux is approximated as,

$$q_{ij} = \frac{\bar{u}^{(j)} - \bar{u}^{(i)}}{R_{ij}} \quad (20)$$

where R_{ij} is the thermal resistance. Empirically, for a component of isotropic heat conductivity k , length ℓ , and cross-section area A , the thermal resistance is $R = \ell/kA$. Between components i and j , define $R_{ij} = R_i + R_j$. In addition, the heat flux due to Dirichlet boundary condition is computed as $q_{iT} = (T_b - \bar{u}^{(i)})/R_i$.

At component i , the dynamics of LCM are given by,

$$\int_{E^{(i)}} \rho c_p \dot{\bar{u}}^{(i)} dE^{(i)} = \left(\sum_{j \in \mathcal{N}_i} \int_{e_{ij}} \frac{\bar{u}^{(j)} - \bar{u}^{(i)}}{R_{ij}} de_{ij} \right) + \int_{e_{iq}} q_b de_{iq} + \int_{e_{iT}} \frac{T_b - \bar{u}^{(i)}}{R_i} de_{iT} \quad (21a)$$

$$\bar{A}^{(i)} \dot{\bar{u}}^{(i)} = \left(\sum_{j \in \mathcal{N}_i} \frac{|e_{ij}|}{R_{ij}} (\bar{u}^{(j)} - \bar{u}^{(i)}) \right) + |e_{iq}| \bar{q}^{(i)} + \frac{|e_{iT}|}{R_i} (\bar{T}^{(i)} - \bar{u}^{(i)}) \quad (21b)$$

$$= \sum_{j \in \mathcal{N}_i} \left(-\frac{|e_{ij}|}{R_{ij}} \bar{u}^{(i)} + \frac{|e_{ij}|}{R_{ij}} \bar{u}^{(j)} \right) + \left(-\frac{|e_{iT}|}{R_i} \bar{u}^{(i)} \right) + \left(|e_{iq}| \bar{q}^{(i)} + \frac{|e_{iT}|}{R_i} \bar{T}^{(i)} \right) \quad (21c)$$

$$= \sum_{j \in \mathcal{N}_i \cup \{T_b\}} \left(\bar{B}_{ij}^{(i)} \bar{u}^{(i)} + \bar{B}_{ij}^{(j)} \bar{u}^{(j)} \right) + \bar{f}^{(i)} \quad (21d)$$

where in eq. (21b) $|e|$ denotes the length ($d = 2$) or area ($d = 3$) of a component boundary e . The $\bar{A}^{(i)}$, $\bar{B}_{ij}^{(i)}$, and $\bar{B}_{ij}^{(j)}$ quantities are provided in ??.

The lumped-mass representation for the four-component TPS is shown in Fig. 2. Let v_i represent the area of the i -th element, $\overline{\rho c_p}_i$, the heat capacity evaluated using the average temperature $\bar{u}^{(i)}$, and $1/R_{ij} = 1/R_i(\bar{u}^{(i)}) + 1/R_j(\bar{u}^{(j)})$ the equivalent thermal resistance between elements i and j . Leveraging the formulas from eqs. (9b) and (10), the LCM matrices are given by,

$$\bar{\mathbf{A}} = \begin{bmatrix} \overline{\rho c_p}_{,1} v_1 & 0 & 0 & 0 \\ 0 & \overline{\rho c_p}_{,2} v_2 & 0 & 0 \\ 0 & 0 & \overline{\rho c_p}_{,3} v_3 & 0 \\ 0 & 0 & 0 & \overline{\rho c_p}_{,4} v_4 \end{bmatrix}, \quad (22a)$$

$$\bar{\mathbf{B}} = \begin{bmatrix} \frac{1}{R_{12}} + \frac{1}{R_{14}} & -\frac{1}{R_{12}} & 0 & -\frac{1}{R_{14}} \\ -\frac{1}{R_{12}} & \frac{1}{R_{12}} + \frac{1}{R_{24}} + \frac{1}{R_{23}} & -\frac{1}{R_{23}} & -\frac{1}{R_{24}} \\ 0 & -\frac{1}{R_{32}} & \frac{1}{R_{32}} + \frac{1}{R_{34}} & -\frac{1}{R_{34}} \\ -\frac{1}{R_{14}} & -\frac{1}{R_{24}} & -\frac{1}{R_{34}} & \frac{1}{R_{14}} + \frac{1}{R_{24}} + \frac{1}{R_{34}} \end{bmatrix}, \quad \bar{\mathbf{f}} = \begin{bmatrix} \bar{q}^{(1)} \\ \bar{q}^{(2)} \\ \bar{q}^{(3)} \\ 0 \end{bmatrix} \quad (22b)$$